

Spatial and Temporal Patterns of Southern Ocean Ventilation

Andrew F. Styles¹, Graeme A. MacGilchrist¹, Michael J. Bell¹, and David P. Marshall¹

¹Affiliation not available

October 17, 2023

Abstract

Ocean ventilation translates atmospheric forcing into the ocean interior. The Southern Ocean is an important ventilation site for heat and carbon and is likely to influence the outcome of anthropogenic climate change. We conduct an extensive backwards-in-time trajectory experiment to identify spatial and temporal patterns of ventilation. Temporally, almost all ventilation occurs between August and November. Spatially, ‘hotspots’ of ventilation account for 60% of open-ocean ventilation on a 30 year timescale; the remaining 40% ventilates in a circumpolar pattern. The densest waters ventilate on the Antarctic shelf, primarily near the Antarctic Peninsula (40%) and the west Ross sea (20%); the remaining 40% is distributed across East Antarctica. Shelf-ventilated waters experience significant densification outside of the mixed layer.

1 **Spatial and Temporal Patterns of Southern Ocean**
2 **Ventilation**

3 **Andrew F. Styles¹, Graeme A. MacGilchrist², Michael J. Bell³, David P.**
4 **Marshall¹**

5 ¹Department of Physics, University of Oxford, Oxford, UK

6 ²Program in Atmospheric and Oceanic Science, Princeton University, Princeton, NJ, USA

7 ³Met Office, Fitzroy Road, Exeter, UK

8 **Key Points:**

- 9 • Extensive backwards-in-time trajectories are used to explore the thirty year his-
10 tory of ventilation in a simulated Southern Ocean
- 11 • Local hotspots only account for a fraction of Southern Ocean ventilation (60%),
12 the remaining ventilation occurs in a circumpolar pattern
- 13 • Almost all Southern Ocean ventilation occurs between August and November while
14 the mixed layer is shoaling

Corresponding author: Andrew F. Styles, afstylesocean@gmail.com

Abstract

Ocean ventilation translates atmospheric forcing into the ocean interior. The Southern Ocean is an important ventilation site for heat and carbon and is likely to influence the outcome of anthropogenic climate change. We conduct an extensive backwards-in-time trajectory experiment to identify spatial and temporal patterns of ventilation. Temporally, almost all ventilation occurs between August and November. Spatially, ‘hotspots’ of ventilation account for 60% of open-ocean ventilation on a 30 year timescale; the remaining 40% ventilates in a circumpolar pattern. The densest waters ventilate on the Antarctic shelf, primarily near the Antarctic Peninsula (40%) and the west Ross sea (20%); the remaining 40% is distributed across East Antarctica. Shelf-ventilated waters experience significant densification outside of the mixed layer.

Plain Language Summary

Only a small fraction of the ocean is interacting with the atmosphere at any given time. This water is definitively found in the upper mixing layer of the ocean. When this water leaves the mixing layer and enters the ocean interior, it has ‘ventilated’ (this term arising from the abundance of oxygen in newly ventilated water). The Southern Ocean is an important region for ventilation, and the uptake of heat and carbon dioxide there is likely to influence the limits and timescales of climate change. By calculating the thirty year history of over 480 million fluid parcels, we find that 60% of open-ocean ventilation occurs in certain ‘hotspots’ and almost exclusively between August and November.

1 Introduction

Ocean ventilation describes how mixed layer properties such as temperature, salinity, and dissolved gas concentrations are translated into the interior ocean. The Southern Ocean is an important area for the ventilation of intermediate and abyssal waters (Gebbie & Huybers, 2010) and is also where much of the deep water formed in the North Atlantic returns to the surface to interact with the atmosphere (Liu & Huang, 2012; Talley, 2013). The ventilation of heat and carbon in the Southern Ocean is expected to influence the limits and timescale of anthropogenic climate change (Bopp et al., 2002; Sallée et al., 2012) and it is therefore important to work out where and when the Southern Ocean ventilates.

Subduction is the transfer of water from the mixed layer into the interior ocean and is often assumed to be a rate-limiting step for Southern Ocean ventilation. Localized subduction ‘hotspots’ can be identified in Argo data (Sallée et al., 2010, 2012) and reanalysis (Buongiorno Nardelli et al., 2018). These sites have deep mixed layers in late winter and undoubtedly influence the ventilation of the Southern Ocean. However, the ventilating effect of subducted water also depends on the timescale of re-entrainment by the mixed layer which is uncertain near these sites (Jones et al., 2016) and can be influenced by ocean currents (Jones et al., 2019). Re-entrained water has no long term influence on the heat (e.g. Frölicher et al., 2015), carbon (Sallée et al., 2010), or nutrient (Sarmiento et al., 2004) budgets of the global interior ocean. Here, we study the spatial and temporal patterns of ventilation using a method that considers the dynamics of subduction and re-entrainment.

Extensive backwards-in-time trajectory experiments reveal the history of the interior ocean including a record of the position and timing of ventilation. For example, MacGilchrist et al. (2020) find that 60% of ventilation in the Labrador Sea occurs within the boundary current and only 20% arises from deep ocean convection. Ventilation sites do not require deep mixed layers when the dynamics of subduction, re-entrainment, and ocean currents are considered. Using similar methodology, MacGilchrist et al. (2021) find that the North Atlantic almost entirely ventilates in late winter, in agreement with the

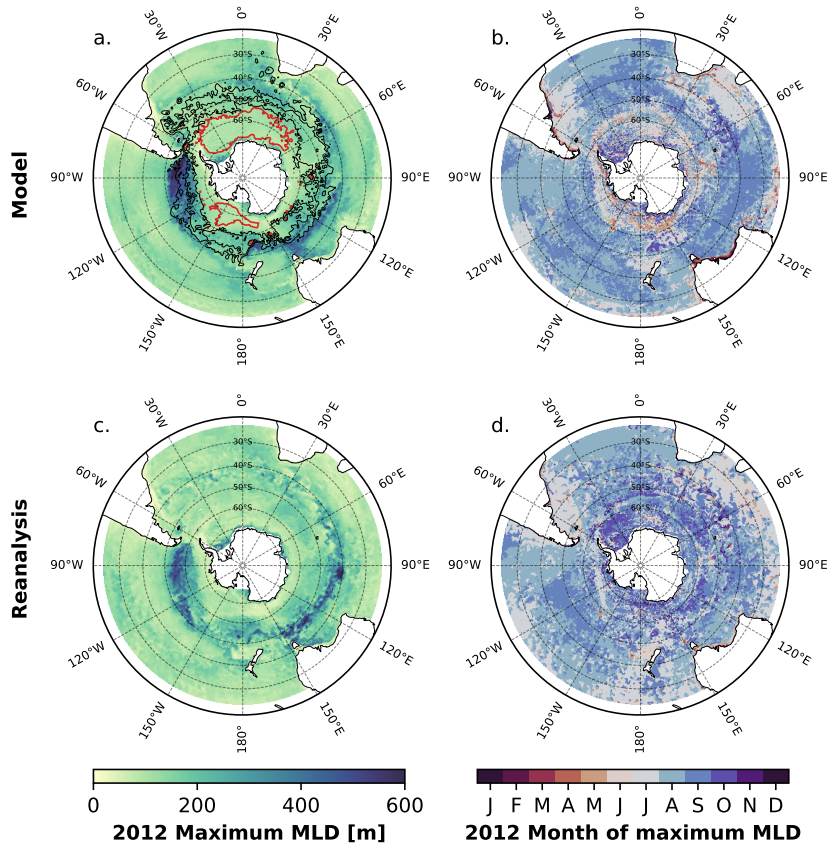


Figure 1. The maximum mixed layer depth (MLD) in 2012 (a) simulated by the forced model and (c) estimated by reanalysis. The timing of the MLD maximum is shown in (b) and (d).

64 earlier passive tracer experiment by Williams et al. (1995) and the theory of ‘Stommel’s
 65 Demon’ (Stommel, 1979). The demon has enabled simpler models of the ocean thermo-
 66 cline, where the base of the late-winter mixed layer is adopted as a non-seasonal upper
 67 boundary (e.g. J. C. Marshall et al., 1993).

68 Figure 1a and 1c show the maximum mixed layer depth (MLD) of the Southern
 69 Ocean in 2012 from a forced model and reanalysis respectively (details are given in Sec-
 70 tion 2). A feature of the MLD in the Southern Ocean is its variation along the Antarc-
 71 tic Circumpolar Current (ACC). The maximum MLD varies between 100 and 500 m along
 72 the ACC’s time-averaged streamlines for 2012 (Figure 1a) and this could influence ven-
 73 tilation timing in the Southern Ocean. Stommel’s demon relies on the net movement of
 74 subducted water to regions with a similar or deeper maximum MLD. In the ACC, wa-
 75 ter that subducts outside of late winter may escape re-entrainment by advecting to an
 76 area with a shallower maximum MLD. It is also possible that the substantial mesoscale
 77 eddy activity of the Southern Ocean will affect the ventilation process (Kwon, 2013; Ka-
 78 menkovich et al., 2017; D. Marshall, 1997; Sallée et al., 2010).

79 We use extensive backwards-in-time trajectories to study the important sites and
 80 timing of all ventilation in the Southern Ocean. We also take the unique opportunity to
 81 compare the properties of shelf-ventilated and off-shelf-ventilated waters using data from
 82 a single experiment.

2 Numerical Simulation and Lagrangian Trajectory Analysis

We use backwards-in-time Lagrangian trajectory analysis in a forced ocean-sea-ice model. Full details of the numerical simulation are given in MacGilchrist et al. (2020) and only essential details are provided here. The numerical simulation is an implementation of the NEMO model (Madec et al., 2019) coupled with the LIM-2 sea-ice model (Bouillon et al., 2009) and was carried out as part of the Drakkar project (Barnier et al., 2006). The ORCA025 configuration is used, which has a horizontal resolution of $1/4^\circ$ (~ 12 km at 65°S and refines with latitude) and 75 irregular vertical model levels. The model is ‘eddy-permitting’, meaning that only the largest mesoscale eddies are resolved. The simulation runs from 1958 to 2015 and is forced with Drakkar Forcing Set 5.2 (Dussin et al., 2016).

Figure 1 compares the forced model to reanalysis from ORAS5 (Zuo et al., 2019) for 2012. The forced model is able to reproduce a similar maximum MLD at a similar time of the year to the observationally-constrained reanalysis. Throughout this study, we define the MLD as the depth where the potential density (reference pressure of 0 dbar) is within 0.01 of the 10 m depth value. The MLD is deep to the west of the Drake Passage and south of Australia and the deepest mixed layers occur between August and September. This is in agreement with previous studies (Buongiorno Nardelli et al., 2017; de Boyer Montégut et al., 2004; Dong et al., 2008; Hanawa & D.Talley, 2001; Sallée et al., 2008, 2010).

The trajectories are calculated using the Lagrangian trajectory code, TRACMASS v7.1 (Aldama-Campino et al., 2020). TRACMASS analytically calculates the trajectory through each model grid cell by assuming that each component of the three dimensional velocity field varies linearly with its respective direction (Blanke & Raynaud, 1997). The trajectories are purely advective and calculated using model velocities that are interpolated between successive 5-day-mean velocity fields. By assuming that the velocity field remains stationary between the intermediate time steps, TRACMASS can calculate approximately mass-conserving trajectories (Döös et al., 2017). NEMO is an incompressible model, so the volume associated with each trajectory is approximately conserved.

We evaluate backwards-in-time trajectories for all interior water that is south of 25°S on the 16th December 2012. Each trajectory has an associated subvolume with a maximum volume of 10^9 m^3 . Over 480 million trajectories are calculated, meaning there are significantly more trajectories than there are grid cells. Backwards-in-time trajectories reveal the history for each of these subvolumes. The earliest point in a subvolume’s history is the most recent occurrence of one of the following:

- it lies in the mixed layer (*Ventilated*);
- it is located north of 25°S ;
- it is more than 30 years old.

In this study, we focus on trajectories with histories starting under the first condition (‘ventilated’ trajectories hereafter). These are the subvolumes that ventilate south of 25°S between 1982 and 2012 and then remain in the ocean interior of this region until the 16th December 2012.

3 Results

In total, 5.80×10^{16} m^3 of water (62 million trajectories) are ventilated in our experiment and Figure 2a shows the age distribution of the ventilated volume. During 2012, the mean MLD is largest in August (Figure 2b) and in our experiment 34% (2.0×10^{16} m^3) of the ventilated volume subducts after this date. These ventilations are ‘short term’ because they may not escape seasonal re-entrainment. The remaining 66% (3.8×10^{16} m^3)

131 of the ventilated volume have escaped re-entrainment. We will be considering the statis-
132 tics of these ‘long term’ ventilations for the remainder of this article.

133 In Figure 2a, there is noticeable inter-annual variability in ventilation which may
134 originate from variations in subduction, re-entrainment or the interior circulation. This
135 suggests that the Southern Ocean is more receptive to surface conditions in specific years
136 of its history. Decadal variability, which may be significant in the Southern Ocean (e.g.
137 Waugh et al., 2013, 2019; Ting & Holzer, 2017), cannot be resolved in our thirty year
138 experiment.

139 Throughout the study, we consider statistics that are aggregated by horizontal po-
140 sition. A single trajectory has two important locations associated with it:

- 141 • their final position: the subvolume’s location on the 16th December 2012,
- 142 • their ventilation position: where the subvolume most recently subducted before
143 the 1st August 2012 (MLD maximum).

144 We use this terminology throughout the article and label all figures with ‘Final’
145 and ‘Vent’ accordingly. There are also two important densities, the potential density at
146 subduction (subduction density hereafter) and the approximate neutral density of the
147 subvolume in its final position (final density hereafter). The neutral density is estimated
148 by calculating approximate neutral density surfaces (ω -surfaces) using the methodology
149 of Stanley et al. (2021). Both the densities use a reference pressure of 0 dbar and agree
150 near the ocean surface.

151 3.1 Stommel’s Demon in the Southern Ocean

152 We find that the timing of ventilation in the Southern Ocean is highly seasonal.
153 In Figure 2b we aggregate all of the ventilated trajectories by their month of ventilation.
154 The majority of subduction occurs between August and November. Everywhere in the
155 Southern Ocean ventilates at approximately the same time of year (Figure 2e). Just like
156 in the North Atlantic (MacGilchrist et al., 2021), the common months of ventilation are
157 when the mixed layer is shoaling. There are so few cases of subduction before July that
158 all sub-regions considered in this study show a similarly seasonal distribution. This is
159 strong evidence that Stommel’s Demon operates in the Southern Ocean.

160 The mean trajectory age for each final horizontal position is shown in Figure 2d.
161 Water in the subpolar gyres is found to be particularly old (over 20 years) towards the
162 center of the gyres. The white spaces in the centre of the gyre inform us that no sub-
163 volumes have ventilated. Figure 2f shows that, compared to the Antarctic margins and
164 the ACC, the gyre basins are poorly ventilated regions when considering a thirty year
165 timescale of ventilation. In Section 3.3, we investigate the partial ventilation of the Wed-
166 dell Gyre.

167 3.2 Ventilation sites and their properties

168 We now aggregate the trajectories by their horizontal location of ventilation to iden-
169 tify the common sites of ventilation and the properties of water that ventilates there. Fig-
170 ure 2g shows the volume ventilated at each ventilation position. There is practically no
171 ventilation within the subpolar gyres and ventilation primarily occurs on the continen-
172 tal shelf or at the northern front of the ACC.

173 In the open ocean, there is circumpolar ventilation along the northern front of the
174 ACC and the zonal symmetry is broken by several ventilation hotspots (Figure 2g). The
175 ventilation hotspots roughly align with subduction hotspots from observational studies
176 (e.g. Sallée et al., 2010, 2012; Buongiorno Nardelli et al., 2018; Morrison et al., 2022) and

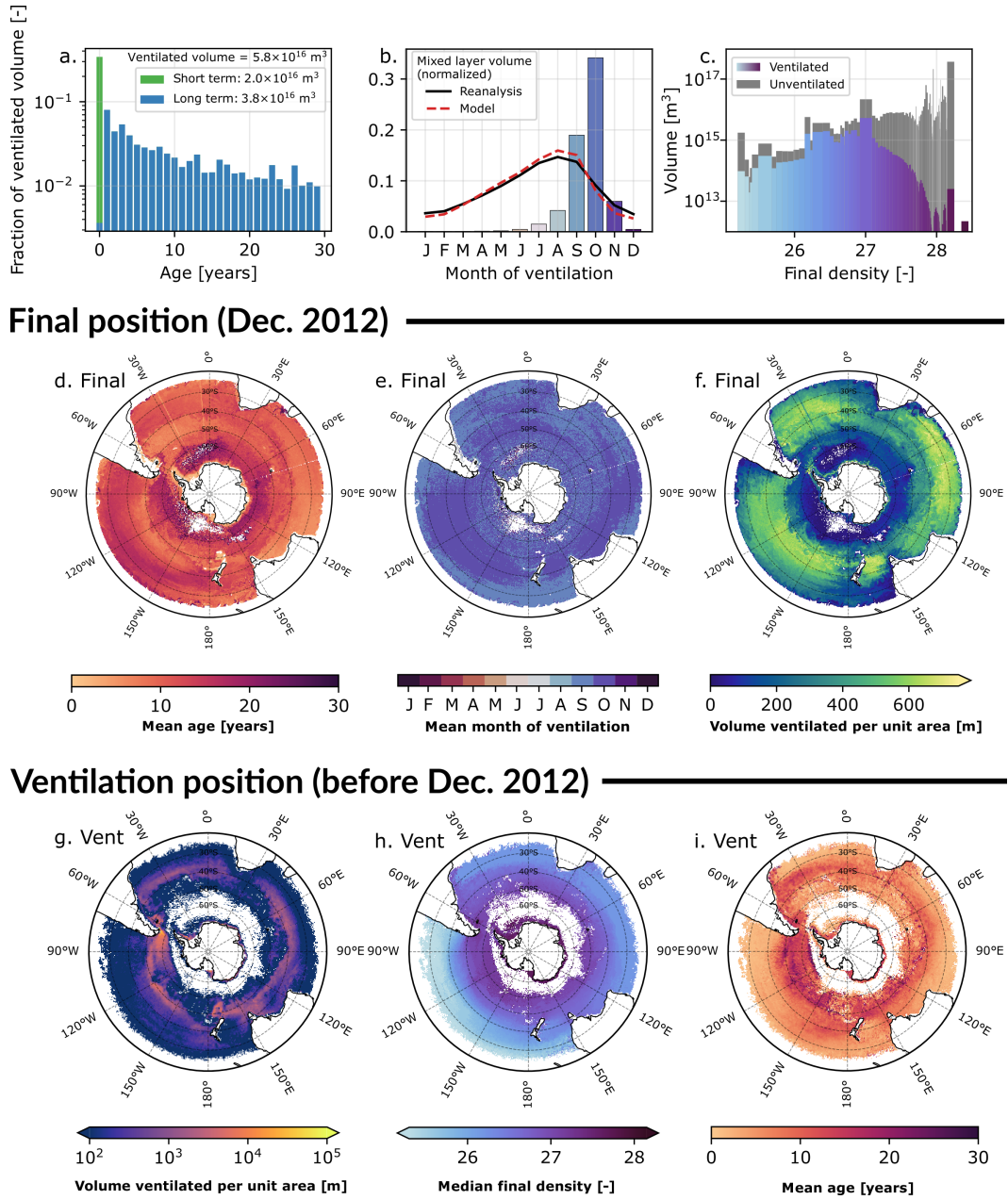


Figure 2. (a) The age distribution of the ventilated trajectories. (b) The ventilated volume aggregated by month and the 2012 mixed layer volume distribution. (c) The ventilated and unventilated volume aggregated by the final density. (d)-(f) The mean age, mean month of ventilation and ventilated volume aggregated by final position. (g)-(i) The ventilated volume, median of the final density, and the mean age aggregated by ventilation position.

177 align with areas of deep convection (Figure 1a). In Section 3.4, we assess the significance
178 of the ventilation hotspots.

179 Figure 2h shows the median final density of the subvolumes based on their venti-
180 lation position. This indicates the eventual density of the water that ventilates at these
181 sites. The lightest water masses ventilate in the Pacific sector and as expected, the dens-
182 est waters in the Southern Ocean ventilate on the Antarctic shelf and the least dense wa-
183 ters ventilate north of the ACC. This result is not trivial since climate models can ex-
184 aggerate the frequency of open-ocean deep-convection events (Heuzé et al., 2015; Reint-
185 ges et al., 2017). The mean age of a subvolume also varies significantly with the loca-
186 tion of ventilation (Figure 2i). Subvolumes that ventilate in areas with deep mixed lay-
187 ers (e.g. west of the Drake Passage) have a mean age between 10 and 20 years. Elsewhere,
188 subvolumes typically have a mean age between 0 and 10 years.

189 3.3 Ventilation of the Weddell Gyre

190 We now only consider trajectories that have a final position within the 10 Sv stream-
191 line of the Weddell Gyre. The two important sites of ventilation are: the Antarctic Shelf
192 and west of the Drake Passage (Figure 3a) where the maximum MLD is deep (Figure
193 1a). Studying both the mean age (Figure 3c) and the average final density (Figure 3d)
194 reveals discrete sources for water of specific density or age in the Weddell Gyre. The youngest
195 waters (5 years or younger) ventilate close to the Weddell Gyre in the southern limits
196 of the Weddell Sea. These young waters have a median final density between 27.5 and
197 27.75. A similarly young population of water also ventilates in the ACC between 150 and
198 90°W. These waters end up as some of the lowest density water masses in the Weddell
199 Gyre interior (approximately 27.25).

200 The densest waters (above 27.75) found in the Weddell Gyre ventilate on the Antarc-
201 tic shelf with a mean age between 10 and 20 years. Similarly dense but much older wa-
202 ter (25-30 years) also ventilate at the site of deep convection west of the Drake Passage
203 (90-60°W).

204 3.4 Ventilation away from the shelf

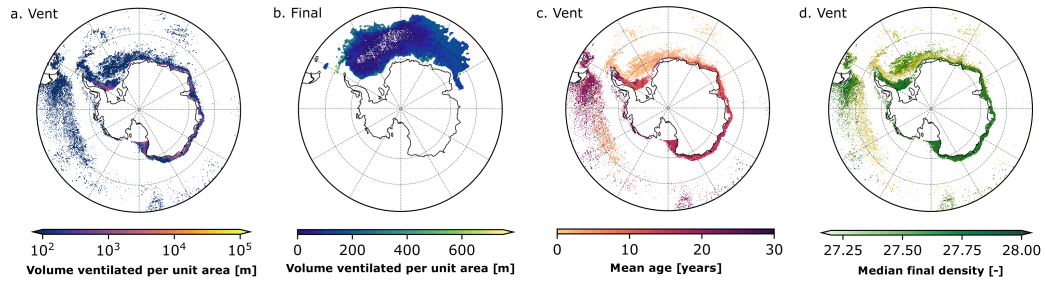
205 We now only consider trajectories that ventilate away from the Antarctic shelf. A
206 trajectory is assumed to have ventilated away from the shelf if its ventilation position
207 is outside the closed 2000m isobath surrounding Antarctica. Figure 3f shows the final
208 distribution of these ventilation subvolumes. Few subvolumes end up in the subpolar gyres
209 or on the shelf. Although there are clear hotspots of ventilation (Figure 3e), the recently
210 subducted water is efficiently spread out across the ACC and north of it, in agreement
211 with Sallée et al. (2010, 2012); Jones et al. (2016).

212 Figure 3h shows how the ventilated volume varies with the longitude of ventilation.
213 Two subduction hotspots dominate the ventilation between 180 and 65°W, where 60%
214 of ventilation occurs. Around the remainder of Antarctica, the hotspots are less appar-
215 ent as ventilation varies smoothly with longitude, suggesting a more circumpolar pat-
216 tern of ventilation. This result suggests that subduction hotspots offer a partial view of
217 open Southern Ocean ventilation.

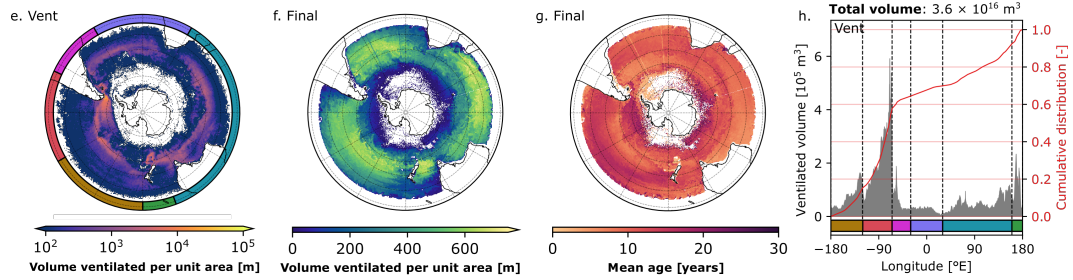
218 3.5 Ventilation on the shelf

219 We now only consider trajectories that ventilate on the Antarctic shelf, within the
220 closed 2000m isobath surrounding Antarctica (Figure 3i). On a thirty year timescale,
221 shelf-ventilated waters are mostly contained south of the ACC but can travel to more
222 northerly latitudes (Figure 3j). In Figure 3k, the youngest subvolumes in the interior ocean
223 are found on the western boundary of the Weddell Gyre (60°W). This region is the most

In the Weddell Gyre (Final position)



Ventilated away from the shelf



Ventilated on the shelf

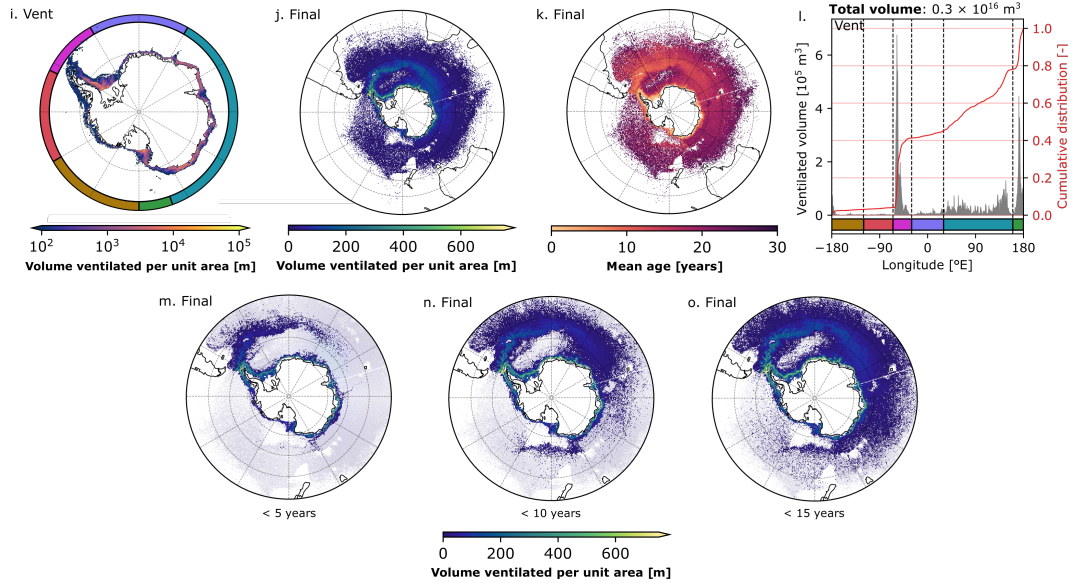


Figure 3. The statistics of ventilated trajectories that have a final position in the Weddell Gyre, ventilated away from the Antarctic shelf, or ventilated on the Antarctic shelf. The gray bars in (h) and (l) show the longitudinal variation of off-shelf and on-shelf ventilated volume respectively. The red line is the cumulative distribution function. The colored bars span the same longitudinal range as the colored arcs in (e) and (i). (m)-(o) the ventilated volume for trajectories that are less than 5, 10, and 15 years old.

224 significant export pathway for shelf-ventilated water. Another weaker pathway follows
 225 the western boundary current of the Ross Gyre. Within five years of ventilating on the
 226 shelf (Figure 3m), some subvolumes have wrapped around the northern limb of the Wed-
 227 dell Gyre and started to traverse the western boundary of the Ross Gyre (160 °E). Within
 228 ten years (Figure 3n), trajectories have started to wrap around the Ross Gyre and be
 229 dispersed by the ACC. Similar export pathways have been found in the passive tracer
 230 experiments of Solodoch et al. (2022).

231 The on-shelf ventilation is more localized than the off-shelf ventilation (Figure 3l).
 232 Approximately 40% of the shelf’s ventilation takes place on the Antarctic Peninsula (65-
 233 30°W) and an additional 20% takes place in the west Ross Sea (160-180°E). These ven-
 234 tilation hotspots align with two of four observed sites of AABW formation on the Antarc-
 235 tic shelf (Purkey et al., 2018). The other two sites (Prydz Bay and the Adélie Coast) are
 236 not clearly pronounced. The remaining 40% of ventilation is evenly spread over East Antarc-
 237 tica (30-160°E). Little ventilation takes place in West Antarctica (180-65°W), which aligns
 238 with the ‘warm shelf’ described in Thompson et al. (2018).

239 3.6 Separability of shelf-ventilated water

240 Almost all of the statistics considered so far have been aggregated by horizontal
 241 position and we have ignored vertical variations. This raises the question, how much over-
 242 lap is there of shelf-ventilated and off-shelf-ventilated water when considering ventila-
 243 tion on a thirty year timescale?

244 Figure 4a shows what fraction of the recorded ventilation in a water column origi-
 245 nates from the Antarctic shelf. Most fluid columns in the Southern Ocean can be ap-
 246 proximated as entirely ventilated on the shelf (100%, blue) or entirely ventilated off the
 247 shelf (0%, red). The interface between these two classes is narrow and aligns closely with
 248 the southern front of the ACC (illustrated by the -10 Sv streamline in Figure 4a). In Sec-
 249 tion 3.5, we found that shelf-ventilated trajectories can travel north of the ACC in 30
 250 years, but Figure 4 suggests that the volume of these trajectories is negligible compared
 251 to the volume of off-shelf-ventilated water.

252 This result highlights the different rates of ventilation for shelf-ventilated and off-
 253 shelf-ventilated water. In thirty years, approximately ten times more water ventilates
 254 in the open ocean ($3.6 \times 10^{16} \text{m}^3$) compared to the Antarctic shelf ($0.3 \times 10^{16} \text{m}^3$), even
 255 though shelf-ventilated abyssal waters make up most of the Southern Ocean (Figure 2c).
 256 A small fraction of the dense water ventilates and is approximately contained south of
 257 the ACC.

258 3.7 Density distribution

259 Finally, we consider the structure of Southern Ocean ventilation in density-latitude
 260 space (Figure 4c-4j). The circumpolar statistics are considered alongside the statistics
 261 of the Atlantic, Indian, and Pacific sectors (Figure 4). Following on from the previous
 262 subsection, a line in density-latitude space separates shelf-ventilated and off-shelf-ventilated
 263 water. The line is not well defined at latitudes greater than 45°S, because so little shelf-
 264 ventilated water reaches this latitude on a thirty year timescale.

265 Most shelf-ventilated water has a final density between 27.25 and 28.00; off-shelf-
 266 ventilated water has a final density between 25.50 and 27.75 (Figure 4d). The densest
 267 shelf-ventilated waters are found in the Atlantic sector (Figure 4f), while the lightest shelf-
 268 ventilated waters are in the Pacific (Figure 4j). Similarly, the lowest density off-shelf-
 269 ventilated waters are found in the Pacific and the highest density subvolumes are found
 270 in the Atlantic. This suggests that the lower density Pacific-ventilated waters (Figure
 271 2h) remain in the Pacific.

272 To understand the trajectory of these volumes in density space, we need to see their
 273 density transformation in the ocean interior. Figure 4b compares the subduction den-
 274 sity to the final density. The central line shows the median subduction density while the
 275 lower and upper lines show the 5th and 95th percentile. These lines represent the enve-
 276 lope of transformation that 90% of the subvolumes experience and the color shows the
 277 shelf water fraction.

278 A fraction of any transformation found in this study may be numerical and could
 279 originate from the following: cumulative errors in the trajectory calculation (van Sebille
 280 et al., 2018), the approximation of neutral density surfaces (Stanley et al., 2021), and
 281 implicit model mixing (Griffies et al., 2000; Lee et al., 2002). Megann (2018) found im-
 282 plicit mixing to be similar to or greater in magnitude than parameterized mixing in a
 283 related NEMO ocean model.

284 Water with a final density less than 27.0 has a similar median subduction density
 285 (Figure 4b). On average, little transformation takes place and the spread of the subduc-
 286 tion density indicates that the range of transformation is within 0.5 of the median. In
 287 contrast, almost all water with a final density greater than 27.0 has become more dense
 288 since subduction. The most extreme cases of densification originate from shelf-ventilated
 289 trajectories with a final density greater than 27.75 and an age greater than 5 years. In
 290 Section 3.3, some of this transformed water is identified in the Weddell Gyre (Figure 3d).
 291 Poorly ventilated dense water and interior densification of lighter water masses indicate
 292 that reserves of denser bottom water are being eroded by interior transformation pro-
 293 cesses. Presumably, the shelf-ventilated waters interact with dense bottom water as they
 294 enter the subpolar gyres and/or follow the ACC (Figure 3n). Studies indicate this may
 295 be happening in the Southern Ocean as a consequence of climate change (e.g. Purkey
 296 & Johnson, 2010; Li et al., 2023; Zhou et al., 2023), but the effect could be exaggerated
 297 by model biases or drifts similar to those found in climate models (Heuzé, 2021; Purich
 298 & England, 2021).

299 4 Conclusions

300 We have used backwards-in-time trajectories to study a thirty year history of the
 301 Southern Ocean and identified spatial and temporal patterns of ventilation that will sim-
 302 plify conceptual models. We found conclusive evidence that ventilation in the Southern
 303 Ocean is highly seasonal. Despite significant variations of the MLD along the stream-
 304 lines of the ACC and significant eddy activity, Stommel’s demon only allows ventilation
 305 between August and November. There is also evidence of inter-annual variability (Fig-
 306 ure 2a); future studies should investigate if an inter-annual demon operates as well us-
 307 ing the methodology of MacGilchrist et al. (2021).

308 We identified spatial patterns of ventilation in the open Southern Ocean. Circum-
 309 polar ventilation takes place along the northern front of the ACC and the zonal sym-
 310 metry is broken by several ventilation hotspots (Figure 2g). The hotspots of ventilation
 311 overlap with sites of deep convection (Figure 1a) and local regions of subduction from
 312 observational studies (Sallée et al., 2010, 2012; Buongiorno Nardelli et al., 2017) but they
 313 only account for 60% of open-ocean ventilation. Circumpolar patterns of ventilation and
 314 ventilation hotspots have similar levels of influence on the Southern Ocean.

315 Almost no ventilation takes place in the subpolar gyres (Figure 2g). Any subduc-
 316 tion that occurs within the streamlines of the gyres is swiftly re-entrained by the follow-
 317 ing mixed layer seasonal cycle. On a thirty year timescale, water in the Weddell Gyre
 318 ventilates remotely. The subvolumes primarily ventilate on the Antarctic shelf but also
 319 ventilate west of the Drake Passage where the mixed layer is deep (Figure 3a).

320 The Antarctic shelf is where the densest water masses of the Southern Ocean ven-
 321 tilate and we find that 40% of shelf ventilation occurs on the Antarctic Peninsula and

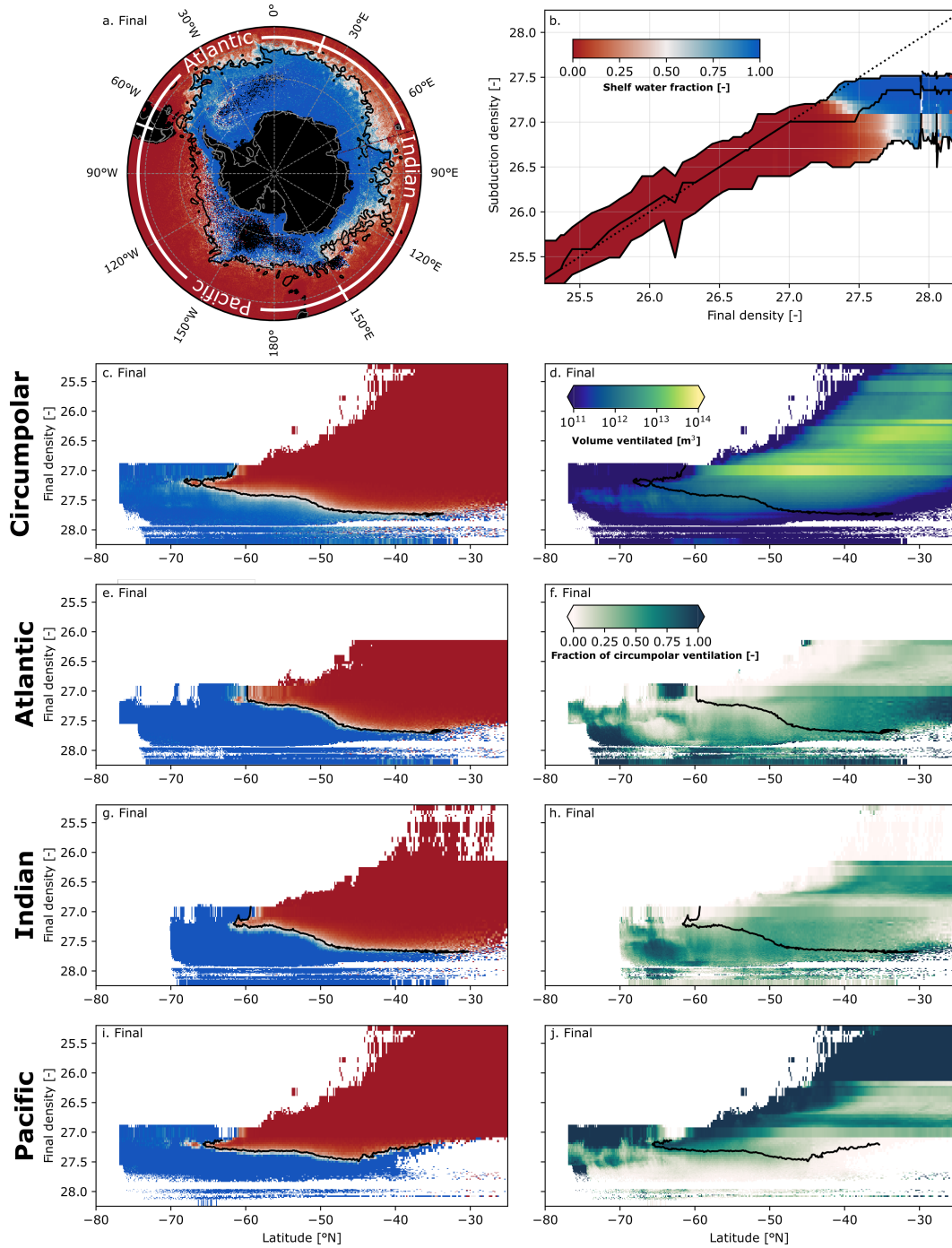


Figure 4. (a) The shelf water fraction aggregated by final position. The black contour is the -10 Sv streamline of the ACC in December 2012. (b) Comparing the subduction density to the final density. The central line shows the median subduction density. The upper and lower lines show the respective 5th and 95th percentile. (c),(e),(g),(i) The shelf water fraction in density-latitude space across various sectors of the Southern Ocean. (d),(f),(h),(j) Ventilation in density-latitude space across the same sectors. The black line in (c)-(j) is the approximate boundary between shelf-ventilated and off-shelf-ventilated waters.

20% in the west Ross sea (Figure 3l). These are two known sites of AABW formation on the Antarctic shelf but other sites are not clear. The remaining 40% of ventilation is spread over East Antarctica. Shelf-ventilated waters are exported to the Southern Ocean via two export pathways, parallel to the western boundaries of the Weddell and Ross Gyre (Figures 3m and 3n) in agreement with passive tracer experiments by Solodoch et al. (2022).

Abyssal waters north of the ACC hardly ventilate on a thirty year timescale (Figure 2c) because shelf-ventilated waters need significantly more time to cross the ACC. In contrast, off-shelf-ventilated waters experience more rapid ventilation in the open Southern Ocean but rarely travel south of the ACC (Figure 2f). Consequently, the southern boundary of the ACC approximately separates columns of shelf-ventilated and off-shelf-ventilated water (Fig 4a). This approximation predicts the area of effect for climate change in the Southern Ocean on anthropogenic timescales. Off-shelf-ventilated waters change quickly over a large area, while denser shelf-ventilated waters modify slowly but accumulate in the smaller area south of the ACC.

Finally, we compared the subduction density to the final density. On average, water with a final density lower than 27.0 experiences little transformation. Almost all water with a final density greater than 27.5 experiences densification after subduction (Figure 4b). This result is consistent with a warming world that is forming less AABW (e.g. Purkey & Johnson, 2010; Li et al., 2023; Zhou et al., 2023) but could be exaggerated by inaccuracies from the eddy-permitting model or the trajectory calculation. Running similar experiments on higher resolution models and reanalysis products may help to determine how realistic this climate change signal is.

Acknowledgments

The work was financially supported by the Natural Environment Research Council NE/S007474/1.

Open Research

Data for the trajectories used in this study are archived on Zenodo (Styles et al., 2023b) alongside the calculated statistics. The software used to analyze the model outputs is also archived on Zenodo (Styles et al., 2023a).

References

- Aldama-Campino, A., Döös, K., Kjellsson, J., & Jönsson, B. (2020, December). *TRACMASS: Formal release of version 7.0*. Zenodo. doi: 10.5281/zenodo.4337926
- Barnier, B., Madec, G., Penduff, T., Molines, J. M., Treguier, A. M., Le Sommer, J., ... De Cuevas, B. (2006). Impact of partial steps and momentum advection schemes in a global ocean circulation model at eddy-permitting resolution. *Ocean Dynamics*, 56(5-6), 543–567. doi: 10.1007/s10236-006-0082-1
- Blanke, B., & Raynaud, S. (1997, June). Kinematics of the Pacific Equatorial Undercurrent: An Eulerian and Lagrangian Approach from GCM Results. *Journal of Physical Oceanography*, 27(6), 1038–1053. doi: 10.1175/1520-0485(1997)027<1038:KOTPEU>2.0.CO;2
- Bopp, L., Le Quéré, C., Heimann, M., Manning, A. C., & Monfray, P. (2002). Climate-induced oceanic oxygen fluxes: Implications for the contemporary carbon budget. *Global Biogeochemical Cycles*, 16(2), 6-1-6-13. doi: 10.1029/2001GB001445
- Bouillon, S., Morales Maqueda, M. Á., Legat, V., & Fichfet, T. (2009, January). An elastic–viscous–plastic sea ice model formulated on Arakawa B and C grids. *Ocean Modelling*, 27(3), 174–184. doi: 10.1016/j.ocemod.2009.01.004

- 370 Buongiorno Nardelli, B., Guinehut, S., Verbrugge, N., Cotroneo, Y., Zambianchi, E.,
 371 & Iudicone, D. (2017). Southern Ocean Mixed-Layer Seasonal and Interannual
 372 Variations From Combined Satellite and In Situ Data. *Journal of Geophysical*
 373 *Research: Oceans*, 122(12), 10042–10060. doi: 10.1002/2017JC013314
- 374 Buongiorno Nardelli, B., Mulet, S., & Iudicone, D. (2018). Three-Dimensional
 375 Ageostrophic Motion and Water Mass Subduction in the Southern Ocean.
 376 *Journal of Geophysical Research: Oceans*, 123(2), 1533–1562. doi: 10.1002/
 377 2017JC013316
- 378 de Boyer Montégut, C., Madec, G., Fischer, A. S., Lazar, A., & Iudicone, D. (2004).
 379 Mixed layer depth over the global ocean: An examination of profile data and a
 380 profile-based climatology. *Journal of Geophysical Research: Oceans*, 109(C12).
 381 doi: 10.1029/2004JC002378
- 382 Dong, S., Sprintall, J., Gille, S. T., & Talley, L. (2008). Southern Ocean mixed-
 383 layer depth from Argo float profiles. *Journal of Geophysical Research: Oceans*,
 384 113(C6). doi: 10.1029/2006JC004051
- 385 Döös, K., Jönsson, B., & Kjellsson, J. (2017, April). Evaluation of oceanic
 386 and atmospheric trajectory schemes in the TRACMASS trajectory model
 387 v6.0. *Geoscientific Model Development*, 10(4), 1733–1749. doi: 10.5194/
 388 gmd-10-1733-2017
- 389 Dussin, R., Barnier, B., Brodeau, L., & Molines, J. M. (2016). *Drakkar forc-*
 390 *ing set DFS5* (Tech. Rep.). Laboratoire de glaciologie et géophysique
 391 de l’environnement. Retrieved from [https://www.drakkar-ocean.eu/
 392 publications/reports/report_DFS5v3_April2016.pdf](https://www.drakkar-ocean.eu/publications/reports/report_DFS5v3_April2016.pdf)
- 393 Frölicher, T. L., Sarmiento, J. L., Paynter, D. J., Dunne, J. P., Krasting, J. P., &
 394 Winton, M. (2015, January). Dominance of the Southern Ocean in Anthro-
 395 pogenic Carbon and Heat Uptake in CMIP5 Models. *Journal of Climate*,
 396 28(2), 862–886. doi: 10.1175/JCLI-D-14-00117.1
- 397 Gebbie, G., & Huybers, P. (2010, August). Total Matrix Intercomparison: A
 398 Method for Determining the Geometry of Water-Mass Pathways. *Journal of*
 399 *Physical Oceanography*, 40(8), 1710–1728. doi: 10.1175/2010JPO4272.1
- 400 Griffies, S. M., Pacanowski, R. C., & Hallberg, R. W. (2000, March). Spu-
 401 rious Diapycnal Mixing Associated with Advection in a z-Coordinate
 402 Ocean Model. *Monthly Weather Review*, 128(3), 538–564. doi: 10.1175/
 403 1520-0493(2000)128<0538:SDMAWA>2.0.CO;2
- 404 Hanawa, K., & D. Talley, L. (2001, January). Chapter 5.4 Mode waters. In
 405 G. Siedler, J. Church, & J. Gould (Eds.), *International Geophysics* (Vol. 77,
 406 pp. 373–386). Academic Press. doi: 10.1016/S0074-6142(01)80129-7
- 407 Heuzé, C. (2021, January). Antarctic Bottom Water and North Atlantic Deep Water
 408 in CMIP6 models. *Ocean Science*, 17(1), 59–90. doi: 10.5194/os-17-59-2021
- 409 Heuzé, C., Ridley, J. K., Calvert, D., Stevens, D. P., & Heywood, K. J. (2015, Octo-
 410 ber). Increasing vertical mixing to reduce Southern Ocean deep convection in
 411 NEMO3.4. *Geoscientific Model Development*, 8(10), 3119–3130. doi: 10.5194/
 412 gmd-8-3119-2015
- 413 Jones, D. C., Boland, E., Meijers, A. J., Forget, G., Josey, S. A., Sallee, J.-B.,
 414 & Shuckburgh, E. (2019). Heat Distribution in the Southeast Pacific
 415 Is Only Weakly Sensitive to High-Latitude Heat Flux and Wind Stress.
 416 *Journal of Geophysical Research: Oceans*, 124(12), 8647–8666. doi:
 417 10.1029/2019JC015460
- 418 Jones, D. C., Meijers, A. J. S., Shuckburgh, E., Sallée, J.-B., Haynes, P., McAufield,
 419 E. K., & Mazloff, M. R. (2016). How does Subantarctic Mode Water venti-
 420 late the Southern Hemisphere subtropics? *Journal of Geophysical Research:*
 421 *Oceans*, 121(9), 6558–6582. doi: 10.1002/2016JC011680
- 422 Kamenkovich, I., Garraffo, Z., Pennel, R., & Fine, R. A. (2017). Importance
 423 of mesoscale eddies and mean circulation in ventilation of the Southern
 424 Ocean. *Journal of Geophysical Research: Oceans*, 122(4), 2724–2741. doi:

- 425 10.1002/2016JC012292
- 426 Kwon, E. Y. (2013). Temporal variability of transformation, formation, and subduc-
427 tion rates of upper Southern Ocean waters. *Journal of Geophysical Research:*
428 *Oceans*, *118*(11), 6285–6302. doi: 10.1002/2013JC008823
- 429 Lee, M.-M., Coward, A. C., & Nurser, A. J. G. (2002, May). Spurious Diapycnal
430 Mixing of the Deep Waters in an Eddy-Permitting Global Ocean Model. *Jour-*
431 *nal of Physical Oceanography*, *32*(5), 1522–1535. doi: 10.1175/1520-0485(2002)
432 032(1522:SDMOTD)2.0.CO;2
- 433 Li, Q., England, M. H., Hogg, A. M., Rintoul, S. R., & Morrison, A. K. (2023,
434 March). Abyssal ocean overturning slowdown and warming driven by Antarctic
435 meltwater. *Nature*, *615*(7954), 841–847. doi: 10.1038/s41586-023-05762-w
- 436 Liu, L. L., & Huang, R. X. (2012, February). The Global Subduction/Obduction
437 Rates: Their Interannual and Decadal Variability. *Journal of Climate*, *25*(4),
438 1096–1115. doi: 10.1175/2011JCLI4228.1
- 439 MacGilchrist, G. A., Johnson, H. L., Lique, C., & Marshall, D. P. (2021). Demons
440 in the North Atlantic: Variability of Deep Ocean Ventilation. *Geophysical Re-*
441 *search Letters*, *48*(9), 1–9. doi: 10.1029/2020GL092340
- 442 MacGilchrist, G. A., Johnson, H. L., Marshall, D. P., Lique, C., Thomas, M.,
443 Jackson, L. C., & Wood, R. A. (2020, December). Locations and Mecha-
444 nisms of Ocean Ventilation in the High-Latitude North Atlantic in an Eddy-
445 Permitting Ocean Model. *Journal of Climate*, *33*(23), 10113–10131. doi:
446 10.1175/JCLI-D-20-0191.1
- 447 Madec, G., Bourdallé-Badie, R., Chanut, J., Samson, E. C., Coward, A., Ethé,
448 C., . . . Samson, G. (2019, October). *NEMO ocean engine*. Zenodo. doi:
449 10.5281/zenodo.1464816
- 450 Marshall, D. (1997). Subduction of water masses in an eddying ocean. *Journal of*
451 *Marine Research*, *55*(2), 201–222. doi: 10.1357/0022240973224373
- 452 Marshall, J. C., Williams, R. G., & Nurser, A. J. G. (1993, July). Inferring the Sub-
453 duction Rate and Period over the North Atlantic. *Journal of Physical Oceanog-*
454 *raphy*, *23*(7), 1315–1329. doi: 10.1175/1520-0485(1993)023(1315:ITSRAP)2.0
455 .CO;2
- 456 Megann, A. (2018, January). Estimating the numerical diapycnal mixing in an eddy-
457 permitting ocean model. *Ocean Modelling*, *121*, 19–33. doi: 10.1016/j.ocemod
458 .2017.11.001
- 459 Morrison, A. K., Waugh, D. W., Hogg, A. M., Jones, D. C., & Abernathy, R. P.
460 (2022). Ventilation of the Southern Ocean Pycnocline. *Annual Review of*
461 *Marine Science*, *14*(1), 405–430. doi: 10.1146/annurev-marine-010419-011012
- 462 Purich, A., & England, M. H. (2021). Historical and Future Projected Warming
463 of Antarctic Shelf Bottom Water in CMIP6 Models. *Geophysical Research Let-*
464 *ters*, *48*(10), e2021GL092752. doi: 10.1029/2021GL092752
- 465 Purkey, S. G., & Johnson, G. C. (2010, December). Warming of Global Abyssal
466 and Deep Southern Ocean Waters between the 1990s and 2000s: Contribu-
467 tions to Global Heat and Sea Level Rise Budgets. *Journal of Climate*, *23*(23),
468 6336–6351. doi: 10.1175/2010JCLI3682.1
- 469 Purkey, S. G., Smethie, W. M., Gebbie, G., Gordon, A. L., Sonnerup, R. E., Warner,
470 M. J., & Bullister, J. L. (2018). A Synoptic View of the Ventilation and
471 Circulation of Antarctic Bottom Water from Chlorofluorocarbons and Nat-
472 ural Tracers. *Annual Review of Marine Science*, *10*(1), 503–527. doi:
473 10.1146/annurev-marine-121916-063414
- 474 Reintges, A., Martin, T., Latif, M., & Park, W. (2017). Physical controls of
475 Southern Ocean deep-convection variability in CMIP5 models and the Kiel
476 Climate Model. *Geophysical Research Letters*, *44*(13), 6951–6958. doi:
477 10.1002/2017GL074087
- 478 Sallée, J.-B., Matear, R. J., Rintoul, S. R., & Lenton, A. (2012, August). Local-
479 ized subduction of anthropogenic carbon dioxide in the Southern Hemisphere

- oceans. *Nature Geoscience*, 5(8), 579–584. doi: 10.1038/ngeo1523
- 480 Sallée, J.-B., Morrow, R., & Speer, K. (2008). Eddy heat diffusion and Subantarctic
481 Mode Water formation. *Geophysical Research Letters*, 35(5). doi: 10.1029/
482 2007GL032827
- 483 Sallée, J.-B., Speer, K., Rintoul, S., & Wijffels, S. (2010, March). Southern Ocean
484 Thermocline Ventilation. *Journal of Physical Oceanography*, 40(3), 509–529.
485 doi: 10.1175/2009JPO4291.1
- 486 Sarmiento, J. L., Gruber, N., Brzezinski, M. A., & Dunne, J. P. (2004, January).
487 High-latitude controls of thermocline nutrients and low latitude biological
488 productivity. *Nature*, 427(6969), 56–60. doi: 10.1038/nature02127
- 489 Solodoch, A., Stewart, A. L., Hogg, A. McC., Morrison, A. K., Kiss, A. E., Thomp-
490 son, A. F., . . . Cimoli, L. (2022). How Does Antarctic Bottom Water Cross
491 the Southern Ocean? *Geophysical Research Letters*, 49(7), e2021GL097211.
492 doi: 10.1029/2021GL097211
- 493 Stanley, G. J., McDougall, T. J., & Barker, P. M. (2021). Algorithmic Improvements
494 to Finding Approximately Neutral Surfaces. *Journal of Advances in Modeling
495 Earth Systems*, 13(5), e2020MS002436. doi: 10.1029/2020MS002436
- 496 Stommel, H. (1979). Determination of water mass properties of water pumped down
497 from the Ekman layer to the geostrophic flow below. *Proceedings of the Na-
498 tional Academy of Sciences*, 76(7), 3051–3055. doi: 10.1073/pnas.76.7.3051
- 499 Styles, A. F., MacGilchrist, G., Bell, M. J., & Marshall, D. P. (2023a, October).
500 *Analysis software for "Spatial and Temporal Patterns of Southern Ocean Ven-
501 tilation"*. Zenodo. doi: 10.5281/zenodo.8413773
- 502 Styles, A. F., MacGilchrist, G., Bell, M. J., & Marshall, D. P. (2023b, October).
503 *Data for "Spatial and Temporal patterns of Southern Ocean Ventilation"*.
504 Zenodo. doi: 10.5281/zenodo.8413705
- 505 Talley, L. (2013, March). Closure of the Global Overturning Circulation Through
506 the Indian, Pacific, and Southern Oceans: Schematics and Transports.
507 *Oceanography*, 26(1), 80–97. doi: 10.5670/oceanog.2013.07
- 508 Thompson, A. F., Stewart, A. L., Spence, P., & Heywood, K. J. (2018). The Antarc-
509 tic Slope Current in a Changing Climate. *Reviews of Geophysics*, 56(4), 741–
510 770. doi: 10.1029/2018RG000624
- 511 Ting, Y.-H., & Holzer, M. (2017). Decadal changes in Southern Ocean ventilation
512 inferred from deconvolutions of repeat hydrographies. *Geophysical Research
513 Letters*, 44(11), 5655–5664. doi: 10.1002/2017GL073788
- 514 van Sebille, E., Griffies, S. M., Abernathy, R., Adams, T. P., Berloff, P., Bi-
515 astoch, A., . . . Zika, J. D. (2018, January). Lagrangian ocean analy-
516 sis: Fundamentals and practices. *Ocean Modelling*, 121, 49–75. doi:
517 10.1016/j.ocemod.2017.11.008
- 518 Waugh, D. W., Hogg, A. M., Spence, P., England, M. H., & Haine, T. W. N. (2019,
519 September). Response of Southern Ocean Ventilation to Changes in Midlati-
520 tude Westerly Winds. *Journal of Climate*, 32(17), 5345–5361. doi: 10.1175/
521 JCLI-D-19-0039.1
- 522 Waugh, D. W., Primeau, F., DeVries, T., & Holzer, M. (2013, February). Recent
523 Changes in the Ventilation of the Southern Oceans. *Science*, 339(6119), 568–
524 570. doi: 10.1126/science.1225411
- 525 Williams, R. G., Marshall, J. C., & Spall, M. A. (1995, December). Does Stom-
526 mel’s Mixed Layer “Demon” Work? *Journal of Physical Oceanography*, 25(12),
527 3089–3102. doi: 10.1175/1520-0485(1995)025<3089:DSMLW>2.0.CO;2
- 528 Zhou, S., Meijers, A. J. S., Meredith, M. P., Abrahamsen, E. P., Holland, P. R., Sil-
529 vano, A., . . . Østerhus, S. (2023, July). Slowdown of Antarctic Bottom Water
530 export driven by climatic wind and sea-ice changes. *Nature Climate Change*,
531 13(7), 701–709. doi: 10.1038/s41558-023-01695-4
- 532 Zuo, H., Balmaseda, M. A., Tietsche, S., Mogensen, K., & Mayer, M. (2019, June).
533 The ECMWF operational ensemble reanalysis–analysis system for ocean and
534

535
536

sea ice: A description of the system and assessment. *Ocean Science*, 15(3),
779–808. doi: 10.5194/os-15-779-2019

537 4066 words 21701 characters (not including spaces)

538 File: Article.tex
539 Encoding: utf8
540 Sum count: 4066
541 Words in text: 3720
542 Words in headers: 49
543 Words outside text (captions, etc.): 282
544 Number of headers: 13
545 Number of floats/tables/figures: 4
546 Number of math inlines: 15
547 Number of math displayed: 0
548 Subcounts:
549 text+headers+captions (#headers/#floats/#inlines/#displayed)
550 166+9+0 (2/0/0/0) _top_
551 541+1+31 (1/1/0/0) Section: Introduction
552 451+6+0 (1/0/3/0) Section: Numerical Simulation and Lagrangian Trajectory Analysis
553 285+1+0 (1/0/10/0) Section: Results
554 193+6+67 (1/1/0/0) Subsection: Stommel's Demon in the Southern Ocean
555 255+5+0 (1/0/0/0) Subsection: Ventilation sites and their properties
556 188+5+85 (1/1/0/0) Subsection: Ventilation of the Weddell Gyre
557 154+5+0 (1/0/0/0) Subsection: Ventilation away from the shelf
558 258+4+0 (1/0/0/0) Subsection: Ventilation on the shelf
559 208+4+0 (1/0/2/0) Subsection: Separability of shelf-ventilated water
560 471+2+99 (1/1/0/0) Subsection: Density distribution
561 550+1+0 (1/0/0/0) Section: Conclusions
562
563 File: output.bbl
564 Encoding: ascii
565 Sum count: 0
566 Words in text: 0
567 Words in headers: 0
568 Words outside text (captions, etc.): 0
569 Number of headers: 0
570 Number of floats/tables/figures: 0
571 Number of math inlines: 0
572 Number of math displayed: 0
573